MARMARA UNIVERSITY
INSTITUTE FOR GRADUATE STUDIES
IN PURE AND APPLIED SCIENCES

SATELLITE ATTITUDE CONTROL WITH THRUSTERS AND REACTION WHEELS IN STATION KEEPING MANEUVER

KEZBAN ÜÇÜNCÜ EMRİ

MASTER THESIS

Department of Electrical and Electronics Engineering

Thesis Supervisor

Assoc. Prof. Onur CİHAN

ISTANBUL, 2021

MARMARA UNIVERSITY
INSTITUTE FOR GRADUATE STUDIES
IN PURE AND APPLIED SCIENCES

SATELLITE ATTITUDE CONTROL WITH THRUSTERS AND REACTION WHEELS IN STATION KEEPING MANEUVER

KEZBAN ÜÇÜNCÜ EMRİ

(525017030)

MASTER THESIS

Department of Electrical and Electronics Engineering

Thesis Supervisor

Assoc. Prof. Onur CİHAN

ISTANBUL, 2021

ACKNOWLEDGEMENT

First of all, I would like to express my deep and sincere gratitude to my supervisor Assoc. Prof. Onur Cihan for his invaluable supervision, support and guidance throughout the study.

I would like to offer my special thanks to Mehmet Burak Ekinci for his valuable comments and suggestions.

I would like to thank my colleagues Yusuf Acar and Dr. Çağatay Yavuzyılmaz for their help during planning of this research work.

I am grateful to my family for their endless support and encouragement throughout my study.

Finally, to my loving and supportive husband, Mehmet: my deepest gratitude. Mehmet, without your help and support this would not have been possible.

July 2021 **Kezban Üçüncü Emri**

CONTENTS

ABSTRACT

SATELLITE ATTITUDE CONTROL WITH THRUSTERS AND REACTION WHEELS IN STATION KEEPING MANEUVER

This thesis presents a control allocation method for momentum management and station-keeping maneuvers simultaneously. The considered satellite model is equipped with internal and external actuators to control the satellite's orbit and attitude and, concurrently, dumping angular momentum stored in the reaction wheels. Our method allocates the external and internal actuators to achieve the control objectives. Internal actuators such as reaction wheels generate torque based on the conservation of the momentum. In this study, two different controllers are utilized to control satellite attitude and reaction wheel speeds. To manage the satellite attitude in three axes, at least three reaction wheels are needed. In this study, four reaction wheels are used to ensure control in case of failure of a reaction wheel. In addition, with six chemical thrusters, east-west and north-south orbit correction maneuvers are performed. For the satellite to serve throughout its service life, fuel optimization of the satellite is required. The proposed control allocation method enforces constraints that maintain orbital accuracy and the satellite in the desired attitude configuration while minimizing the use of thrusters and significantly reducing fuel consumption. The method combines two generally separated objectives of orbital and attitude control through constraints determined by the propulsion system. Presented numerical simulations show that the proposed control allocation method significantly increases the service life of geostationary satellites.

ÖZET

MEVZİ KORUMA MANEVRASINDA İTİCİ VE TEPKİ TEKERİ İLE UYDU YÖNELİM KONTROLÜ

Bu tezde yerdurağan yörüngedeki bir uydunun eşzamanlı olarak yörünge düzeltmesi ve momentum yönetimi yapabilmesi için bir kontrol dağıtım yöntemi önerilmektedir. Ele alınan uydu modeli, uydunun yönelimini ve yörüngesini kontrol etmesi ve aynı zamanda tepki tekerlerinde depolanan açısal momentumu boşaltmak için koordine edilmesi gereken içsel ve dışsal eyleyiciler ile donatılmıştır. Yöntem, kontrol hedeflerine ulaşmak için içsel ve dışsal eyleyicilerin birleşiminin nasıl dağıtıldığını gösterir. Tepki/momentum tekerleri gibi iç eyleyiciler momentumun korunmasına dayalı tork üretirler. Bu çalışmada uydu yönelimini ve tepki tekeri hızlarını kontrol eden iki farklı kontrolcü tasarlanmıştır. Uydu yöneliminin üç eksende kontrol edilebilmesi için en az 3 adet tepki tekerine ihtiyaç vardır. Bu çalışmada herhangi bir tekerin arızalanması durumunda kontrolün sağlanabilmesi için dört adet tepki tekeri kullanılmıştır. Buna ek olarak, kullanılan altı adet kimyasal itici ile Doğu-Batı ve Kuzey-Güney yörünge düzeltme manevraları yapılabilmektedir. Uydunun görev ömrü boyunca hizmet verebilmesi için uydudaki yakıt kullanımının optimize edilmesi gerekir. Önerilen kontrol dağıtım yöntemi, iticilerin kullanımını en aza indirerek yakıt tüketimini önemli ölçüde azaltırken, yörünge doğruluğu ve ayakucu noktasını işaret eden bir yönelim yapılandırmasında uyduyu koruyan kısıtlamaları uygulamaktadır. Yöntem, yörünge ve yönelim kontrolünün genellikle ayrıştırılmış iki hedefini tahrik sistemi üzerindeki belirlenen kısıtlamalar yoluyla birleştirir. Önerilen yöntemi doğrulamak için sayısal simülasyonlar gerçekleştirilmiştir. Yapılan simülasyonlar, önerilen kontrol dağıtım yönteminin kullanılmasının yerdurağan uyduların hizmet ömrünü önemli ölçüde arttırabileceğini göstermektedir.

SYMBOLS

$\vec{\mathbf{a}}_{\mathbf{moon}}$: Lunar perturbation acceleration vector (km/s^2)

$\vec{\mathbf{a}}_{\mathbf{sun}}$: Solar perturbation acceleration vector (km/s^2)

$\vec{\mathbf{a}}_{\mathbf{p}}$: Total perturbation acceleration vector (km/s^2)

$\widehat{\mathbf{A}}^{(\mathbf{b,t})}$: Attitude matrix that transforms coordinates from F_t to F_b

$\mathbf{A_u}$: Allocation matrix

$\mathbf{b}$: SCA constant

$\bar{\mathbf{e}}$: Euler unit vector

$\mathbf{F}$: Force generated in the maneuver direction F_x or F_y (N)

$\mathbf{F_{max}}$: Maximum allowable thrust (N)

$\bar{\mathbf{F}}_{\mathbf{t}}^{(\mathbf{b})}$: Thruster forces expressed in F_b (N)

$\mathbf{F_b}$: Body frame

$\mathbf{F_e}$: ECEF frame

$\mathbf{F_i}$: ECI frame

$\mathbf{F_t}$: Target frame

$\bar{\mathbf{H}}_{\mathbf{w}}^{(\mathbf{b})}$: Angular momentum of the reaction wheels along their spin axes (kgm^2/s)

$\hat{\mathbf{J}}_{\mathbf{s}}^{(\mathbf{b})}$: Moment of inertia of the satellite (kg/m^2)

$\mathbf{J_{wi}}$: i-th reaction wheel moment of inertia (kg/m^2)

$\mathbf{k}$: Current iteration

$\mathbf{K}$: Maximum number of iterations

$\mathbf{K_d}$: Attitude controller derivative gain

$\mathbf{K_{i,w}}$: Wheel speed controller integral gain

$\mathbf{K_g}$: Attitude controller gain

$\mathbf{K_p}$: Attitude controller proportional gain

$\mathbf{K_{p,w}}$: Wheel speed controller proportional gain

$\mathbf{K_{t,w}}$: Wheel speed controller anti-windup gain

$\mathbf{m}$: Satellite mass (kg)

$\boldsymbol{\mu}$: Earth's gravitational constant (km^3/s^2)

$\boldsymbol{\mu_{moon}}$: Lunar gravitational constant (km^3/s^2)

$\boldsymbol{\mu_{sun}}$: Solar gravitational constant (km^3/s^2)

$\mathbf{n_{wheel}}$: Number of the reaction wheel

$\mathbf{w_{wi/b}}$: Angular velocity of the i-th reaction wheel in spin axes with respect to F_b (rad/s)

$\tilde{\mathbf{w}}_{\mathbf{b/i}}^{\mathbf{(b)}}$: Cross product matrix of $\bar{w}_{b/i}^{(b)}$

$\boldsymbol{\Omega}$: Skew symmetric matrix

$\bar{\mathbf{q}}$: Attitude quaternion

$\bar{\mathbf{q}}_{\mathbf{err}}^{\mathbf{(b/i)}}$: Saturated quaternion error of F_b with respect to F_i

$\mathbf{P_i^t}$: Position of the destination point in i-th dimension at t-th iteration

$\bar{\mathbf{r}}^{\mathbf{(i)}}$: Satellite position in F_i (km)

$\mathbf{r_1, r_2, r_3, r_4}$: Random numbers

$\bar{\mathbf{r}}_{\mathbf{moon}}^{\mathbf{(i)}}$: Position of the moon (km)

$\bar{\mathbf{r}}_{\mathbf{sun}}^{\mathbf{(i)}}$: Position of the sun (km)

$\bar{\mathbf{r}}_{\mathbf{ti}}^{\mathbf{(b)}}$: Position of the i-th thruster in F_b (m)

$\mathbf{T_s}$: Attitude controller settling time

$\bar{\mathbf{T}}_{\mathbf{t}}^{\mathbf{(b)}}$: Torques provided by thrusters in F_b (Nm)

$\bar{\mathbf{T}}_{\mathbf{w}}^{(\mathbf{b})}$: Reaction wheel torques in F_b (Nm)

$\mathbf{u}$: Desired thrust vector

$\bar{\mathbf{u}}_{\mathbf{c}}^{(\mathbf{b})}$: Control torque in F_b (Nm)

$\bar{\mathbf{u}}_{\mathbf{wi}}^{(\mathbf{b})}$: Unit vector of the i-th reaction wheel in F_b

$\bar{\mathbf{u}}_{\mathbf{ti}}^{(\mathbf{b})}$: Unit vector of the i-th thruster in F_b

$\bar{\mathbf{v}}^{(\mathbf{i})}$: Satellite velocity vector in F_i (km/s)

$\boldsymbol{\vartheta}$: Angle of rotation

$\mathbf{X}_{\mathbf{i}}^{\mathbf{t}}$: Position of the current solution in i-th dimension at t-th iteration

$\boldsymbol{\xi}$: Damping ratio

ABBREVIATIONS

CoM : Center of Mass

ECI : Earth-Centered Inertial

ECEF : Earth-Centered/Earth-Fixed

GEO : Geostationary Earth Orbit

IP : Integral Proportional

PD : Proportional Derivative

OOP : On-Orbit Propagator

RW : Reaction Wheel

SCA : Sine Cosine Algorithm

LIST OF FIGURES

LIST OF TABLES

1 INTRODUCTION

1.1 Background

Satellites with the same orbital period as the rotation period of Earth are referred to as geosynchronous satellites. They return to the same position after each sidereal day. Orbits of Geostationary Earth Orbit (GEO) satellites are along a path parallel to Earth's rotation. While all geostationary satellites are geosynchronous, some geosynchronous satellites may not be geostationary. Geostationary satellite orbit lies over the equator. Therefore, they seem fixed as they move at the same angular velocity as Earth. The ground track of the geostationary satellites is stable. They are pointed at a particular place on the ground to provide coverage to that area. They can cover a wide range of the globe. GEO satellites located at an altitude of about 36,000 km have a lifespan of 10-15 years. They are used to provide voice communication, the internet, and TV broadcasting. Since their orbit lies over the equator, it is difficult for them to broadcast near the polar region.

GEO satellites are subjected to various non-Keplerian forces and disturbance torques constantly, resulting in a deviation from the satellite's desired orbital position (Bong-Kyu Park et al., 2005). For satellites in GEO, the fundamental perturbations are solar and lunar gravitational attractions that induce drift in orbital inclination, solar radiation pressure that affects orbit eccentricity (Losa, 2007). Therefore, to prevent these perturbations while maintaining satellite attitude, station-keeping maneuvers are required. Station-keeping maneuvers include a series of orbit correction maneuvers implemented by the electrical thrusters (Weiss et al., 2018; Satpute and Emami, 2019). To compensate for the solar and lunar gravitational attractions, keeping the inclination to the equatorial plane is needed. This is provided by the north/south maneuver. Besides, the east/west maneuver is performed to keep the satellite in the longitude window in the nominal station-keeping maneuver plan. The east/west maneuver controls the orbit eccentricity. **Figure 1.1** presents an example of nominal longitude window and control limits. Otherwise, these perturbations would drive the satellite out of its assigned slot. The commonly used station-keeping maneuver technique is shown in **Figure 1.2**.

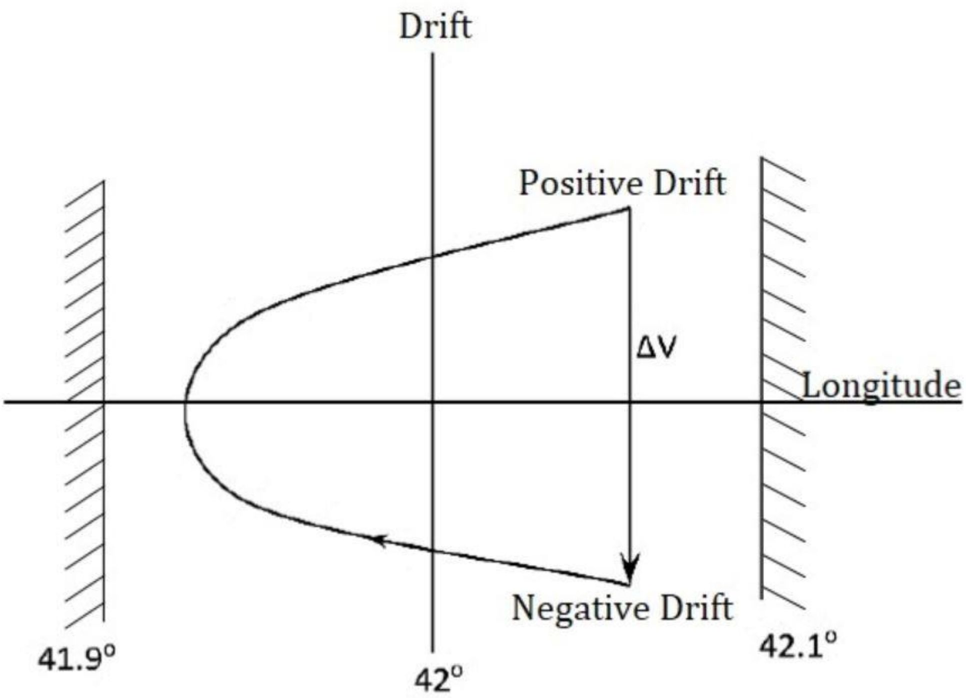

Figure 1.1 Sample of longitude window (42° east)

As can be seen from **Figure 1.2**, in an example maneuver cycle, first the north/south maneuver and then the east/west maneuver are performed. On the other hand, the precise orbit of the satellite calculated on the ground is uploaded to the satellite before the north/south maneuver. This process is called OOP (On-Orbit Propagator) Update (Yılmaz, 2016). The time and frequency of this operation may differ depending on the satellite platform or manufacturer.

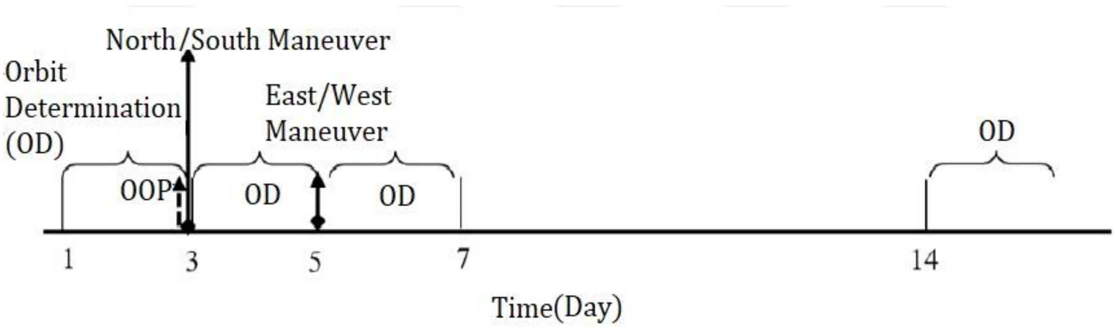

Figure 1.2 Station-keeping maneuver cycle plan

The north/south maneuver is done 3-4 days before the east/west maneuver. Thus, the errors that may arise from the north/south maneuver are prevented from growing exponentially. East/west maneuver is a corrective maneuver including these effects performed (Maral, G. et al., 2009). **Figure 1.1** shows the change in drift direction by adding a linear velocity ΔV to the satellite drifting eastward. After this maneuver, the satellite begins to shift westward. However, since the eastward force continues, it accelerates again in the same direction after a while.

GEO satellites are ideally located within a window of typically ±0.1° from the equatorial plane. North/South maneuver is performed at ascending or descending nodes to maintain the angle between the orbit plane and the ecliptic plane. As can be seen from **Figure 1.3**, the North/South maneuver is performed at the elevation point by adding a ΔV perpendicular to the orbital plane. The old and new trajectories in this state are shown in **Figure 1.3**. The fuel consumed by the satellite in the North maneuver in a month is approximately equivalent to the fuel consumption in the east in one year. Therefore, these maneuvers are planned very precisely.

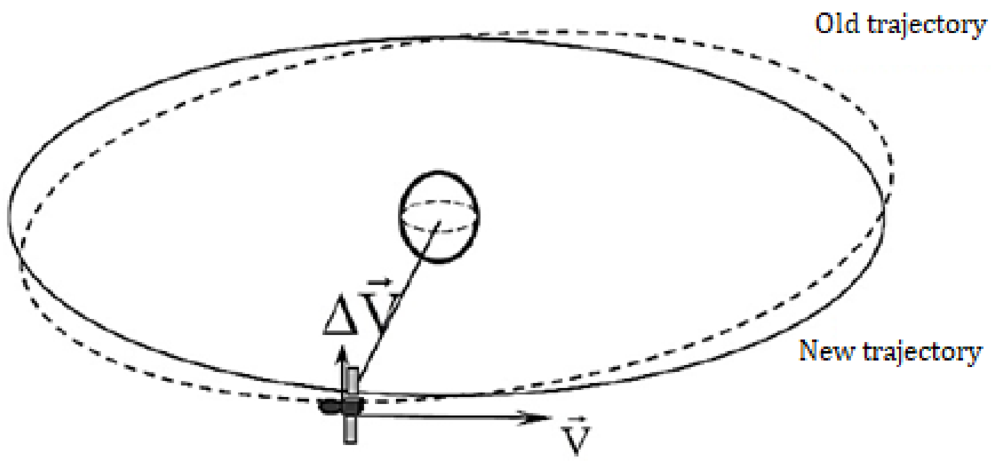

Figure 1.3 North/South Maneuver

In the east maneuver, the velocity ΔV is added to the satellite moving along the drift with the linear velocity V. In this case, the satellite accelerates and moves into a higher orbit, thus shifting west relative to the Earth. **Figure 1.4** shows the GEO satellite orbit before and after an example east maneuver. With the east/west maneuver, the orbital period is controlled and ensured satellite in the longitude window.

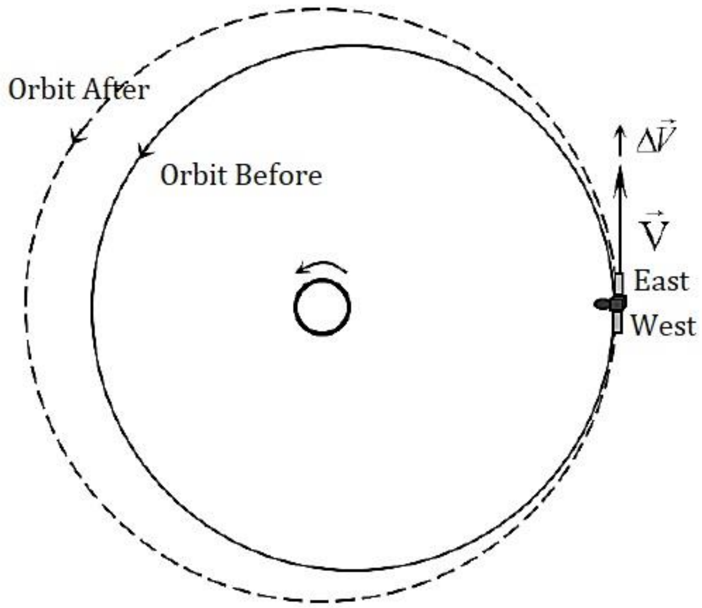

Figure 1.4 East Maneuver

Thrusters are significant actuators for station-keeping maneuvers. They are used for both attitude and orbit control of the GEO satellite. Usage of electric propulsion has become preferable thanks to the increased power level of the GEO satellites. Therefore, the orbit raising from transfer orbits to GEO is performed with electric thrusters. Electric propulsion provides a greater payload compared to chemical propulsion in GEO satellites. Although the electric propulsion system appears to be a viable alternative due to the critical reduction in satellite mass, they produce relatively low thrust compared to chemical propulsion. For this reason, orbit transfers require electrical thrusters firing nearly continuously for weeks or even months. (Kimbrel, 2002). However, the main problem with this kind of application is that electric propulsion can achieve much higher specific impulses than chemical propulsion. Chemical thrusters generate higher thrust with lower specific impulses. Therefore, they can rarely fire for short periods when implementing station-keeping maneuvers. A short thrust period is sufficient for the ΔV required to perform these maneuvers. Electric thrusters, however, provide low thrust at high specific impulses. Thus, they must fire for long periods to manage the same ΔV as chemical thrusters (Thomas, 2016). Consequently, an electric propulsion system is generally not preferred for conventional station-keeping strategies. Presently, most GEO satellites are equipped with chemical thrusters.

Thruster redundancy is a significant issue in the GEO satellites and plays a key role in orbit control. The satellite reliability is increased by using redundant thrusters in case some of the main thrusters fail. A previous study (Jin et al., 2006) suggested a method for efficient chemical thruster redundancy. (Rex and Köhnecket, 2012) provided important information on electric propulsion redundant configurations. They presented several thruster configurations and analyzed these configurations according to nominal and redundant operating modes. (Barissov et al., 2015) discussed the degradation of the thruster response and propose the station keeping strategy for performing the reliable east/west and north/south maneuvers.

In the literature, numerous studies have attempted to explain station-keeping techniques. (Chao and Baker, 1983) discussed orbit propagation and station-keeping maneuver of GEO satellites. (Guelman, 2014) examined real-time closed-loop orbit control for station-keeping of the GEO satellites with electric thrusters, without taking the perturbations and the optimization of the thrusters' usage into account. (Shrivastava, 1978) investigated station-keeping methods and perturbation environments in GEO satellites. Furthermore, (Frederik J. de Bruijn, 2016) presented a method that can be used for station-keeping with a convex optimization technique. The method is generic and can be applied to both chemical and electrical propulsion systems. It is aimed to minimize fuel consumption with thruster optimization. (Emma and Pernicka, 2003) proposed a three-phase algorithm that combines longitude control and eccentricity control autonomously. (Losa, 2007) focused on comparing station-keeping maneuver planning methods for geostationary satellites equipped with electrical and chemical thrusters. Previous studies have not been able to show that momentum management and attitude control of the nadir pointing satellite. (Weiss et al., 2018) discussed the model predictive control strategy for concurrent station-keeping and momentum management of GEO satellites with electrical thrust. To better understand the model predictive control policy and its effects, (Weiss et al., 2018) pointed out numerical simulations. In the same vein, (Satpute and Emami, 2019) suggested a convex optimization algorithm for minimize fuel consumption while a momentum management maneuver. (Jin et al.,

2006) proposed a control allocation problem for the redundant thrusters. This constrained optimization problem is solved by a built-in MATLAB function. Together these studies provided important insights into station-keeping and momentum management of GEO satellites with electrical thrust. (Thopil, 2006) suggested two controllers, and examined the thruster control performance. Propellant requirement for station-keeping maneuvers is also calculated in this study. Momentum management is performed by magnetic torque rods. Satellite angular velocity is estimated by estimation methods that are generally used.

1.2 Concept

GEO satellites perturb from environmental torques that disturb the satellite attitude. Reaction wheels can be used to counteract the effects of disturbing torques. Therefore, momentum management is required periodically to overcome these torques. To sustain the satellite attitude, the disturbing torques must be absorbed by the reaction wheels. The satellite attitude should be managed by using at least three reaction wheels in three axes.

Reaction wheels cannot rotate at randomly high speeds and begin to saturate after a while. Therefore, the momentum reserved by the reaction wheels have to disposed by using thrusters. (Tsiotras et al., 2001) attempted to explain the momentum management of four-momentum wheels. They also proposed the power-tracking method for attitude control. In this study, thrusters are used for torque implementation for maneuvers. (Ismail, Z. and Varatharajoo, R., 2009) proposed the two configuration sets of the reaction wheels for three axis attitude control of the satellite. Momentum management of the reaction wheels and attitude control performances are presented in this study. The usage of thrusters needs to be optimized to minimize the fuel consumption of satellites since one of the most significant factors affecting satellite life span is fuel consumption.

In this thesis, we use convex quadratic and population-based optimization algorithms for unloading momentum of GEO satellites for station-keeping purposes. Population-based optimization algorithm ensures the attitude controller performance, and the convex optimization method is used for thruster optimization. To generate the concurrent reaction wheel momentum control and station-keeping maneuver, orbital and attitude dynamics are considered simultaneously. The satellite with realistic thruster and reaction wheel configurations are discussed for the applicability of the proposed method. We believe that no other authors have studied orbit correction and momentum unloading maneuvers with chemical thrusters concurrently. This thesis therefore set out to assess the simultaneously station-keeping and momentum management using chemical thrusters.

1.3 Contributions of the Thesis

The proposed method in this thesis allows the controller to

1. keep the satellite in the desired attitude configuration,
2. maintain the satellite in a station-keeping box,
3. keep the angular velocity of the reaction wheels within the saturation limits,
4. unload the reserved angular momentum from the reaction wheels,
5. minimize the fuel consumption with the proposed optimization algorithm.

1.4 Organization of the Thesis

Throughout the structure of the study composed of five chapters, including this introduction chapter.

Chapter 2 starts by laying out the theoretical dimensions of the thesis and examines how to model the kinematics and dynamics of the satellite. A description of each model is presented. This chapter includes the actuators used for the concurrent station-keeping and momentum unloading maneuvers simulations.

The third chapter is concerned with the attitude and wheel speed controller policy. Input-output relations are given. This chapter provides a formulation of optimization problems to minimize the fuel consumption and maintain the satellite in the station-keeping box and not exceeding the saturation limits. The proposed optimization techniques are used for attitude controller and thruster allocation.

Chapter 4 shows the findings of the thesis, concentrating on verifying the proposed control allocation method.

The final chapter draws together the various strands of the thesis. A summary and critique of the results are given in this chapter.

2 MATHEMATICAL MODELS AND ACTUATORS

2.1 Notation Preliminaries

In this thesis, we denote an arbitrary reference frame a with F_a. The term $\overline{w}_{a/b}^{(c)}$ is used solely when referring to the angular velocity of F_a with respect to F_b, expressed in F_c. $\overline{x}^{(a)}$ denotes the column matrix representation of $\vec{x}$ expressed in F_a (for further information, see (Özgören, 2007)).

2.2 Reference Frames

The position and velocity or attitude of the satellite are defined with several reference frames. The most significant reference frames are the Earth-Centered Inertial Frame (ECI), Earth-Centered/Earth-Fixed Frame, the Body Frame, and the Target Frame.

2.2.1 Earth-Centered inertial frame

Earth-Centered Inertial Frame (ECI), denoted by F_i, can be represented by the axes triple $\{i_1, i_2, i_3\}$ where i_1 axis is aligned with the mean vernal equinox, i_3 axis is pointing towards the mean North pole, and the cross product of i_1 and i_3 is the i_2 axis. As shown in **Figure 2.1**, i_1 is pointing towards the intersection of the vernal equinox and equator. The vernal equinox is fixed at some specific epoch (Vallado, 2001).

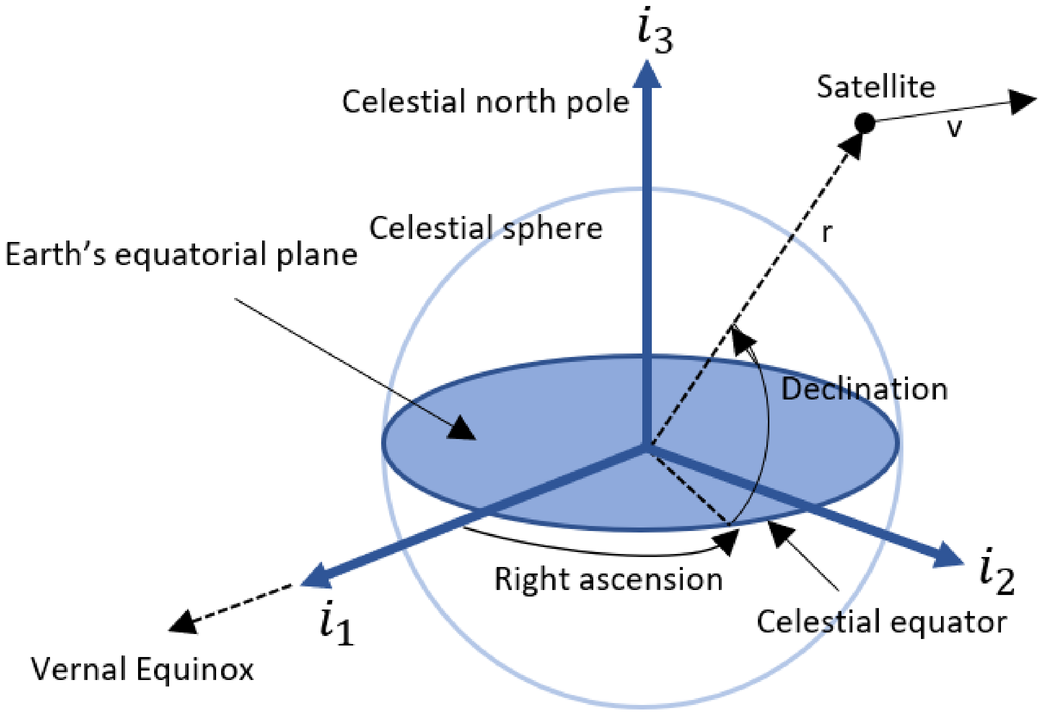

Figure 2.1 ECI Frame

2.2.2 Earth-Centered/Earth-Fixed frame

The Earth-Centered/Earth-Fixed (ECEF) Frame, denoted by F_e, can be represented by the axes triple $\{e_1,e_2,e_3\}$ as shown in **Figure 2.2**. Its i_3 axis is identical with the ECI frame $e_3=i_3$ which is given in Section 2.2.1. The coordinates of the target point on the Earth are defined in F_e.

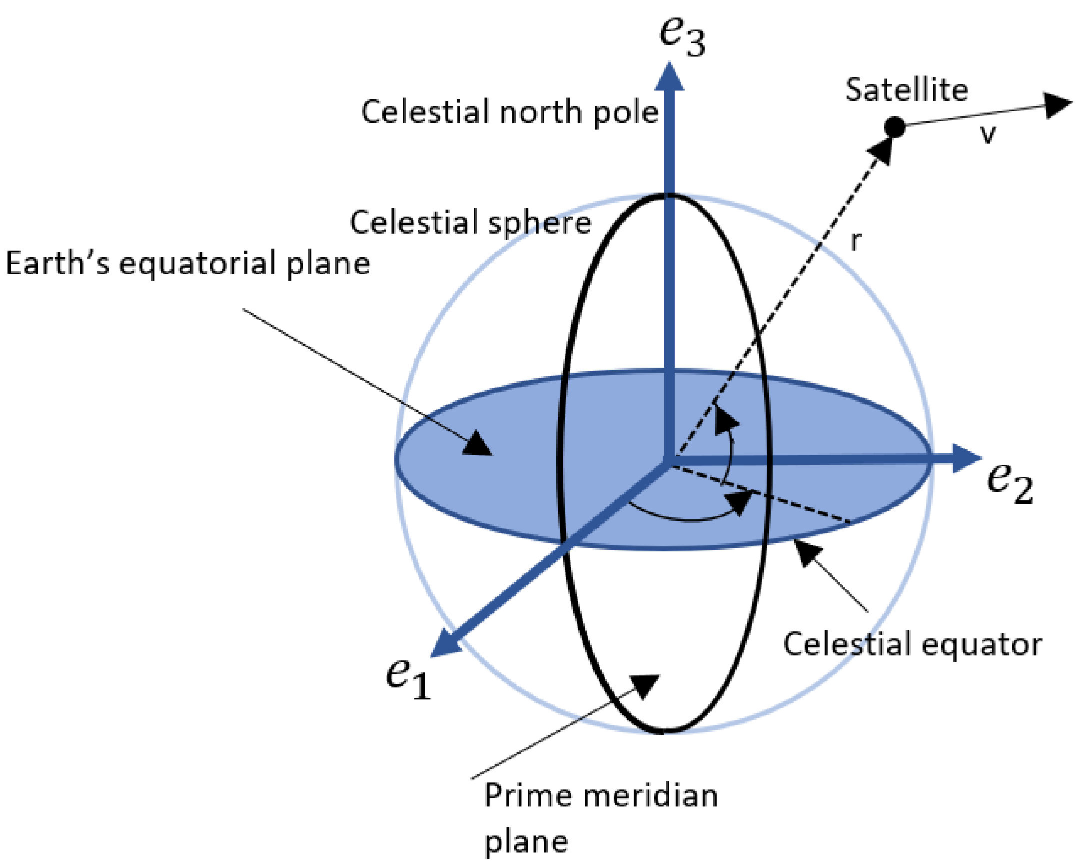

Figure 2.2 ECEF Frame

2.2.3 Body frame

The body frame is described by an origin at the center of mass (CoM) of the satellite and three Cartesian axes, which are shown in **Figure 2.3**. Its b_1 axis is aligned with the east panel of the satellite, the b_2 axis is aligned with the south panel of the satellite, and the b_3 axis is aligned with the apogee motor of the satellite.

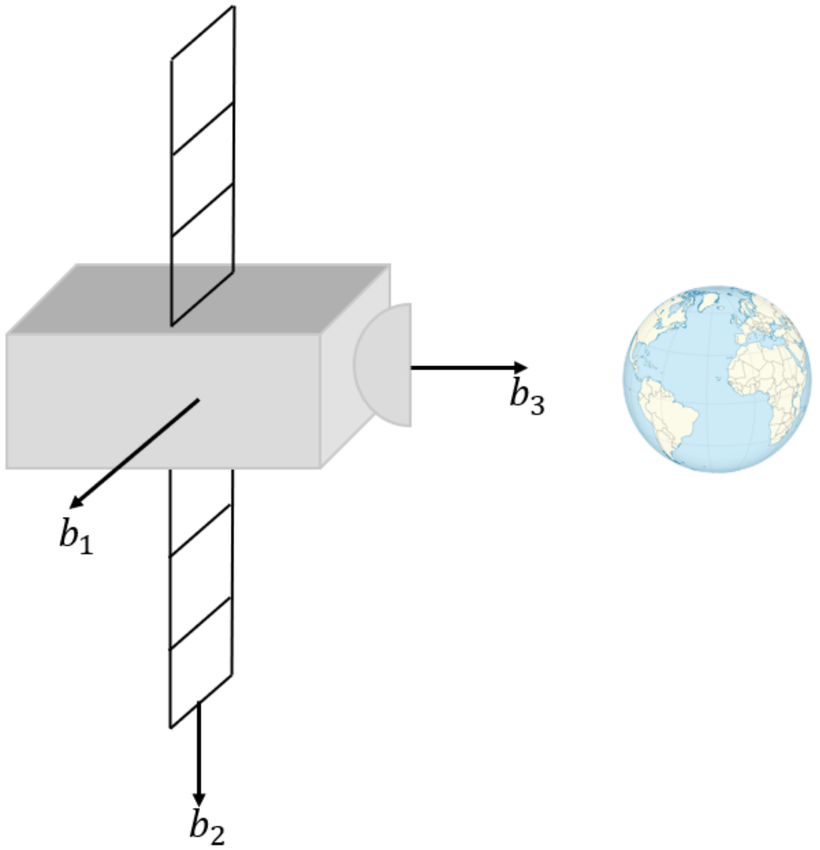

Figure 2.3 Body Frame

2.2.4 Target frame

The GEO satellite aims to broadcast to a specific region on the Earth's surface in the station-keeping maneuvers, Thus, the satellite is controlled according to the reference frame defined about a target on the Earth. Thanks to this frame, the broadcast area can be kept constant despite the orbit inclination and the movements of the Earth axis. Therefore, the reference frame is chosen as F_t which is represented by the axes triple $\{t_1,t_2,t_3\}$ as shown in **Figure 2.4**. Note that the t_3 axis of the target frame is pointing to the target point. The t_1 axis is aligned with the velocity vector. The cross product of the t_1 and t_3 axes is the t_2 axis which is opposite to the orbital plane normal. The t_1 axis is normal to the position vector and positive in the direction of the velocity vector.

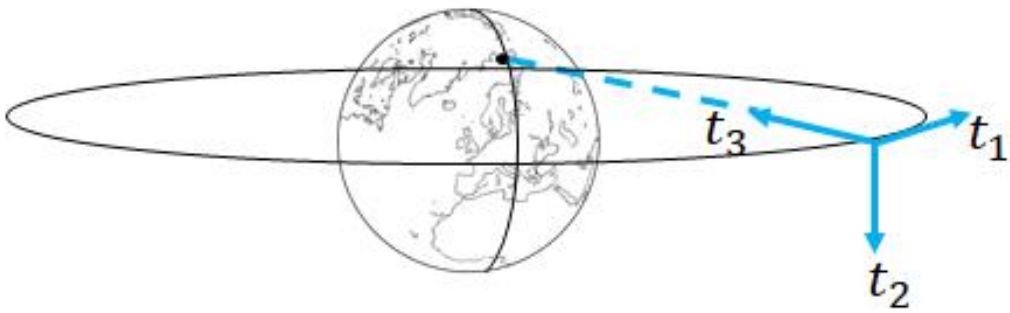

Figure 2.4 Target Frame

2.3 Attitude Representations

Leonhard Euler is considered as one of the most significant mathematicians of the 18th century and one of the leading mathematicians of all time, who laid the foundations for the analysis of rotations. In his rotation theorem, Leonhard Euler states that any rearrangement of a rigid body such that a point on the rigid body lasts fixed is a rotation about a fixed axis (called Euler axis) (Wertz, 1998). The representation of rotation in three dimensions is expressed with at least three parameters. There are several representation methods. Euler angle and quaternion representations are the two most preferred methods. The advantages and disadvantages of these two significant representations are summarized in **Table 2.1**. As can be seen from the table, the quaternion is more efficient than Euler angles for a satellite attitude analysis because quaternion representation is not required any trigonometric functions.

Table 2.1 Euler Angle and Quaternion Attitude Representations Comparison

Representation	Euler Representation	Quaternion Representation
Advantages	• More intuitive • Easy to interpret physically	• No singularity problem • No required trigonometric functions • Easy to interpolate between rotations
Disadvantages	• Singular • Changes suddenly in response to small change in rotation	• No clear physical interpretation

2.3.1 Euler angle representation

The Euler angle representation is used to represent vector transforms from one frame to another frame. The transformation of the vector is fulfilled with three consecutive rotations about different axes. Three rotation matrices are used for describing these rotations. The rotation matrices consist of the Euler angles.

There are twelve sets of Euler parameters, six of which is symmetric and six of which is asymmetric. Six symmetric sets are: 1-2-1, 1-3-1, 2-3-2, 2-1-2, 2-3-2, 3-1-3, and 3-2-3 whereas six asymmetric sets are 1-2-3, 1-3-2, 2-3-1, 2-1-3, 3-1-2, and 3-2-1. The three angles in an asymmetric Euler angle sequence are generally referred to as roll, pitch, and yaw. In this thesis, the roll, pitch, and yaw angles are assigned to indices 1, 2, and 3, respectively. In this thesis, the Euler 2-1-3 sequence is preferred. This sequence means pitch(θ)→roll(ϕ)→yaw(ψ) rotation order y, x, and z axes. The rotation matrices related with the pitch, roll and yaw rotations are denoted by $\widehat{A}_2$, $\widehat{A}_1$ and $\widehat{A}_3$; and can be expressed as

$$\widehat{A}_2=\begin{bmatrix} c\theta & 0 & -s\theta \\ 0 & 1 & 0 \\ s\theta & 0 & c\theta \end{bmatrix} \qquad (2.1)$$

$$\hat{A}_1=\begin{bmatrix}1 & 0 & 0\\ 0 & c\phi & s\phi\\ 0 & -s\phi & c\phi\end{bmatrix} \tag{2.2}$$

$$\hat{A}_3=\begin{bmatrix}c\psi & s\psi & 0\\ -s\psi & c\psi & 0\\ 0 & 0 & 1\end{bmatrix} \tag{2.3}$$

The product of these three rotation matrices is called the attitude matrix, which is an orthogonal matrix given by

$$\hat{A}_{213}(\psi,\theta,\phi)=\hat{A}_2\hat{A}_1\hat{A}_3=\begin{bmatrix}c\phi c\psi+s\phi s\theta s\psi & c\theta s\psi & -s\phi c\psi+c\phi s\theta s\psi\\ -c\phi s\psi+s\phi s\theta c\psi & c\theta c\psi & s\phi s\psi+c\phi s\theta c\psi\\ s\phi c\theta & -s\theta & c\phi c\theta\end{bmatrix} \tag{2.4}$$

where c(.) and s(.) are cosine and sinus functions, respectively. $\hat{A}_{213}$ can be used for transformation from the reference frame F_r to the body frame F_b.

2.3.2 Quaternion representation

The quaternion, denoted by $\bar{q}=[q_1,q_2,q_3,q_4]^T$ is a four-element vector which is particularly useful in studying attitude representation. $\bar{e}=[e_1,e_2,e_3,e_4]^T$ is the vector along the direction of the rotation. Each component of $\bar{q}$ is defined by functions of vector $\bar{e}$ and magnitude of the rotation ϑ given as

$$q_1=e_1\sin\frac{\vartheta}{2} \tag{2.5}$$

$$q_2=e_2\sin\frac{\vartheta}{2} \tag{2.6}$$

$$q_3=e_3\sin\frac{\vartheta}{2} \tag{2.7}$$

$$q_4 = e_4 \cos\frac{\vartheta}{2} \tag{2.8}$$

The quaternion product matrix is

$$[\bar{q}\otimes] = \begin{bmatrix} q_4 & q_3 & -q_2 & q_1 \\ -q_3 & q_4 & q_1 & q_2 \\ q_2 & -q_1 & q_4 & q_3 \\ -q_1 & -q_2 & -q_3 & q_4 \end{bmatrix} \tag{2.9}$$

The complex conjugate of $\bar{q}$ can be expressed as $\bar{q}^* = [-q_1, -q_2, -q_3, -q_4]^T$ and the quaternion representation of the attitude matrix is given by

$$\widehat{A}(q) = \begin{bmatrix} q_1^2 - q_2^2 - q_3^2 + q_4^2 & 2(q_1 q_2 + q_3 q_4) & 2(q_1 q_3 - q_2 q_4) \\ 2(q_1 q_2 - q_3 q_4) & -q_1^2 + q_2^2 - q_3^2 + q_4^2 & 2(q_2 q_3 + q_1 q_4) \\ 2(q_1 q_3 + q_2 q_4) & 2(q_2 q_3 - q_1 q_4) & -q_1^2 - q_2^2 + q_3^2 + q_4^2 \end{bmatrix} \tag{2.10}$$

Throughout the thesis, we use both $\widehat{A}_{213}(\psi, \theta, \phi)$ and $\widehat{A}(q)$ to denote the attitude matrix.

2.4 GEO Satellite Dynamics

The fundamental equations of the orbital and attitude dynamics of the satellite are discussed in this section.

2.4.1 Orbital dynamics

The orbit model which will be further utilized to describe satellite motion is considered in this section. The nonlinear equation of motion of the satellite is given by

$$\ddot{\bar{r}}^{(i)} = -\mu \frac{\bar{r}^{(i)}}{r^3} + \frac{1}{m} \bar{F}_t^{(b)} + \vec{a}_p \tag{2.11}$$

where μ is the Earth's gravitational constant, m is the mass of the satellite, $\bar{F}_t^{(b)}$ is the external forces applied to the satellite by the thrusters, $\bar{r}^{(i)}$ is the satellite position vector in the inertial frame (ECI, F_i) and $\vec{a}_p$ is the total perturbation acceleration. Common perturbations are non-spherical central body, solar radiation pressure, and moon and sun gravitational interactions (Curtis, 2010). The main perturbations are the lunar and solar gravitational attractions which are formulated as

$$\begin{aligned}
\vec{a}_{moon} &= \mu_{moon}\left(\frac{\bar{r}_{moon}^{(i)}-\bar{r}^{(i)}}{\left|\bar{r}_{moon}^{(i)}-\bar{r}^{(i)}\right|^3}-\frac{\bar{r}_{moon}^{(i)}}{\left|\bar{r}_{moon}^{(i)}\right|^3}\right)\\
\vec{a}_{sun} &= \mu_{sun}\left(\frac{\bar{r}_{sun}^{(i)}-\bar{r}^{(i)}}{\left|\bar{r}_{sun}^{(i)}-\bar{r}^{(i)}\right|^3}-\frac{\bar{r}_{sun}^{(i)}}{\left|\bar{r}_{sun}^{(i)}\right|^3}\right)\\
\vec{a}_p &= \vec{a}_{moon}+\vec{a}_{sun}
\end{aligned} \tag{2.12}$$

where μ_{moon} and μ_{sun} are the lunar and solar gravitational constants, respectively; $\bar{r}_{moon}^{(i)}$ and $\bar{r}_{sun}^{(i)}$ are the positions of the moon and sun, respectively. The Orbit model converts the target position in F_e to F_i since the Guidance algorithm needs to the target position in F_i.

2.4.2 Attitude dynamics with reaction wheels

The satellite rigid body attitude dynamics is actuated by the reaction wheels. The equation of motion for the attitude dynamics of the satellite can be expressed in body fixed frame F_b as

$$\dot{\bar{w}}_{b/i}^{(b)}=\hat{J}_s^{(b)^{-1}}\left[\bar{T}_t^{(b)}-\bar{T}_w^{(b)}-\tilde{w}_{b/i}^{(b)}(\hat{J}_s^{(b)}\bar{w}_{b/i}^{(b)}+\sum_{i=1}^{n_{wheel}} J_{wi}\, w_{wi/b}\bar{u}_{wi}^{(b)})\right] \tag{2.13}$$

where $\dot{\bar{w}}_{b/i}^{(b)}$ is the derivative of the angular velocity vector in F_b with respect to F_I, expressed in F_b; $\hat{J}_s^{(b)}$ and J_{wi} are the satellite inertia and i-th reaction wheel inertia, respectively. $\vec{T}_t^{(b)}$ and $\vec{T}_w^{(b)}$ are the torques provided by thrusters and reaction wheels' torque vectors, respectively. $w_{wi/b}$ is the angular velocity of the i-th reaction wheel in spin axes. n_{wheel} is the number of the reaction wheels in the satellite and $\bar{u}_{wi}^{(b)}$ is the unit vector of the i-th reaction wheel. The unit vectors corresponding to the reaction wheels of the satellite model considered in the thesis are given by

$$\bar{u}_{w1}{}^{(b)}=\frac{1}{\sqrt{3}}\begin{bmatrix}1\\1\\1\end{bmatrix},\ \bar{u}_{w2}{}^{(b)}=\frac{1}{\sqrt{3}}\begin{bmatrix}1\\1\\-1\end{bmatrix},$$

$$\bar{u}_{w3}{}^{(b)}=\frac{1}{\sqrt{3}}\begin{bmatrix}-1\\1\\-1\end{bmatrix},\ \bar{u}_{w4}{}^{(b)}=\frac{1}{\sqrt{3}}\begin{bmatrix}-1\\1\\1\end{bmatrix} \tag{2.14}$$

2.5 GEO Satellite Kinematics

In this section, the kinematics of the attitude is discussed. In this thesis, the attitude of the satellite is represented by a quaternion, which leads to the following representation for the attitude kinematics (Markley and Crassidis, 2014)

$$\dot{\bar{q}}^{(b/i)}(t)=\frac{1}{2}\Omega\left(\bar{w}_{b/i}{}^{(b)}(t)\right)\bar{q}^{(b/i)}(t) \tag{2.15}$$

Here, $\Omega(\bar{w}_{b/i}{}^{(b)})$ is a skew symmetric matrix expressed as

$$\Omega\left(\bar{w}_{b/i}{}^{(b)}\right)=\begin{bmatrix}0 & w_z & -w_y & w_x\\ -w_z & 0 & w_x & w_y\\ w_y & -w_x & 0 & w_z\\ -w_x & -w_y & -w_z & 0\end{bmatrix}. \tag{2.16}$$

where the angular velocity vector in F_b with respect to inertial frame F_i, expressed in F_b is stated separately as $\bar{w}_{b/i}{}^{(b)}=[w_x \quad w_y \quad w_z]^T$.

Substituting Equation (2.16) into Equation (2.15) gives

$$\dot{q}_1{}^{(b/i)}=\frac{1}{2}\left[w_z q_2-w_y q_3+w_x q_4\right] \tag{2.17}$$

$$\dot{q}_2{}^{(b/i)}=\frac{1}{2}\left[-w_z q_1+w_x q_3+w_y q_4\right] \tag{2.18}$$

$$\dot{q}_3^{(b/i)}=\frac{1}{2}\left[w_y q_1 - w_x q_2 + w_z q_4\right] \quad (2.19)$$

$$\dot{q}_4^{(b/i)}=\frac{1}{2}\left[-w_x q_1 - w_y q_2 - w_z q_3\right] \quad (2.20)$$

2.6 Functional Architecture

In this thesis, system design is composed of six sections. **Figure 2.5** illustrates the functional architecture of the system whose details are given in the following sections.

Orbit block calculates the current satellite position and velocity, whereas Dynamics block contains the dynamical equations related with the motion of the satellite and generates reaction wheel speed, angular velocity, and attitude of the satellite. Guidance block computes the attitude and angular velocity in the desired reference frame which are the inputs of the Attitude Controller block. The Attitude Controller block calculates the desired torque by not exceeding the maximum tolerable attitude error. Thruster Allocation block solves the optimum thruster usage problem. Finally, the Wheel Speed Controller block controls the reaction wheel speed for momentum unloading of the reaction wheels.

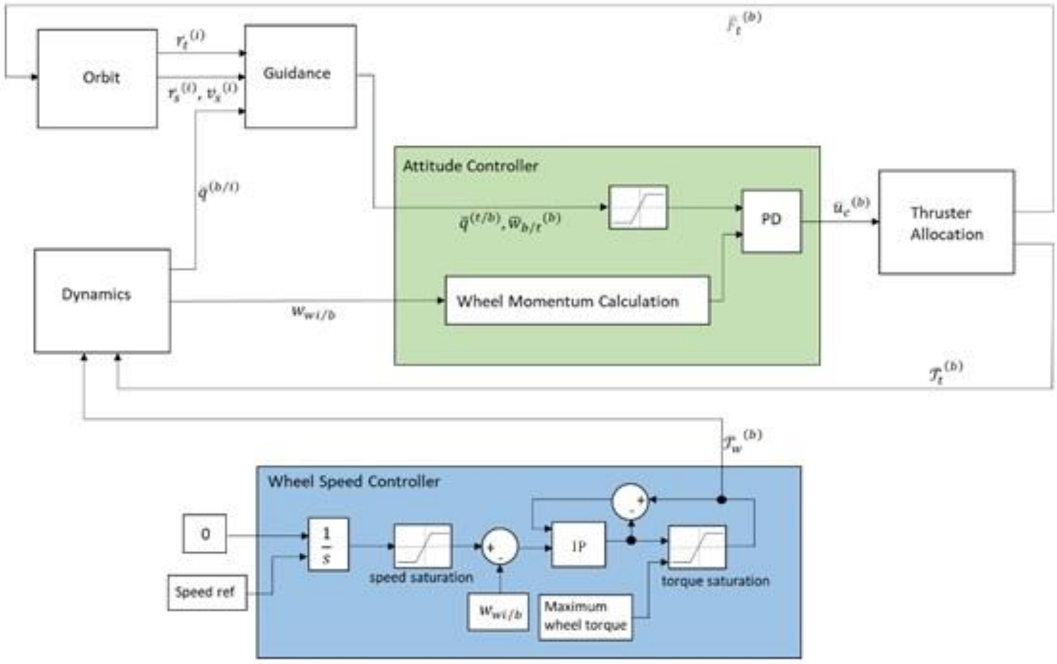

Figure 2.1 Functional architecture of the system

2.7 Actuators

2.7.1 Reaction wheels

Actuators play a significant role in delivering the control motions of the satellites. Reaction wheels are essential attitude control actuators for GEO satellites. They control the attitude of the satellite with high precision. The reaction wheels transfer the momentum to the satellite for attitude control. A minimum of three reaction wheels is required for control of the satellite in three axes. In the system under consideration, four reaction wheels are used. There are two popular four-reaction wheel configurations. These configurations are pyramid and NASA standard configuration (Markley and Crassidis, 2014). In this thesis, it is assumed that the reaction wheels are placed in a square pyramidal structure and symmetry on each coordinate plane which allows them, to generate torque in all directions. **Figure 2.6** illustrates the configuration of the reaction wheels. This arrangement provides to increase momentum storage and torque capability. The surface normal of the square-based pyramid is the momentum axes of the reaction wheels.

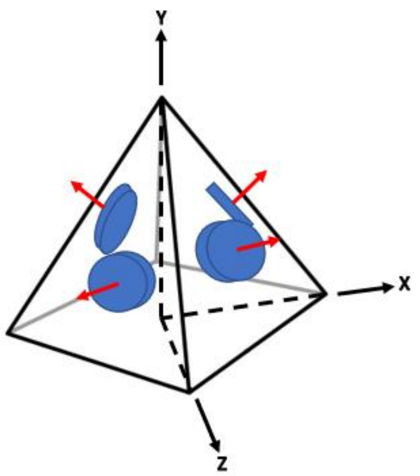

Figure 2.6 Square based pyramid structure used in reaction wheel configuration

Maximum torque and maximum rotational speed capabilities of the reaction wheels are varied. In this thesis, the torque range of the reaction wheels is ±0.22 Nm, the rotational speed range is ±4500 rpm. It is assumed that all reaction wheels on the satellite are identical in this study.

2.7.2 Chemical thrusters

Thrusters are used for both orbit and attitude control of the satellites since they generate both forces and torques. In momentum unloading maneuvers, thrusters are the main actuators. Satellites have limited propellant supply which makes the usage of chemical thrusters disadvantageous in GEO satellites. The proposed control allocation method in the thesis minimizes propellant consumption.

We consider a satellite consisting of six thrusters whose placement is depicted in **Figure 2.7**. Thrusters are distributed over the satellite's north, east and west panels which allows the torque to be applied in any direction and the force to be applied in +x, -x and -y directions. Thus, orbit correction is planned regarding available force directions.

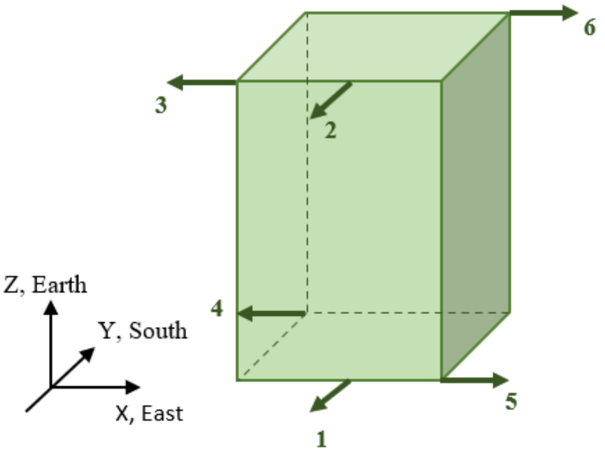

Figure 2.7 Placement of the thrusters

The unit vectors of the six thrusters in F_b are presented in **Table 2.2**.

Table 2.2 Unit vector of the thruster

Thruster	Unit vector	Thruster	Unit vector	Thruster	Unit vector
1	$\bar{u}_{t1}^{(b)} = \begin{bmatrix} 0 \\ 1 \\ 0 \end{bmatrix}$	3	$\bar{u}_{t3}^{(b)} = \begin{bmatrix} 1 \\ 0 \\ 0 \end{bmatrix}$	5	$\bar{u}_{t5}^{(b)} = \begin{bmatrix} -1 \\ 0 \\ 0 \end{bmatrix}$
2	$\bar{u}_{t2}^{(b)} = \begin{bmatrix} 0 \\ 1 \\ 0 \end{bmatrix}$	4	$\bar{u}_{t4}^{(b)} = \begin{bmatrix} 1 \\ 0 \\ 0 \end{bmatrix}$	6	$\bar{u}_{t6}^{(b)} = \begin{bmatrix} -1 \\ 0 \\ 0 \end{bmatrix}$

3 CONTROLLER DESIGN

3.1 Guidance Algorithm

In GEO, satellites can be controlled according to target frame F_t which is referenced to the satellite's orbit. The Guidance algorithm calculates $\bar{q}^{(t/i)}$, $\bar{q}^{(t/b)}$,$\bar{w}_{b/t}{}^{(b)}$ and $\bar{w}_{t/i}{}^{(t)}$. Using the satellite position $\vec{r}^{(i)}$ and velocity $\vec{v}^{(i)}$ vectors that are calculated in the Orbit model in F_i, $\bar{q}^{(t/i)}$ can be extracted from the attitude matrix. $\bar{q}^{(b/i)}$ is calculated by using the attitude kinematics. $\bar{q}^{(t/b)}$ is quaternion error between $\bar{q}^{(b/i)}$ and $\bar{q}^{(t/i)}$ which is calculated from $\bar{q}^{*}$and Equation (2.10) as

$$\bar{q}^{(t/b)}=[\bar{q}^{(b/i)}\otimes]\ \bar{q}^{*\,(t/i)} \tag{3.1}$$

Furthermore, $\bar{w}_{b/t}{}^{(b)}$ is obtained from

$$\bar{w}_{b/t}{}^{(b)}= \bar{w}_{b/i}{}^{(b)}-\widehat{A}^{(b,t)}\bar{w}_{t/i}{}^{(t)}. \tag{3.2}$$

where $\bar{w}_{b/t}{}^{(b)}$ indicates the angular velocity in body frame F_b with respect to the target frame F_t, expressed in F_b where $\bar{w}_{b/i}{}^{(b)}$ is obtained from the attitude dynamics equations, $\bar{w}_{t/i}{}^{(t)}$ is a function of $\dot{\bar{q}}^{(t/i)}$, and $\widehat{A}^{(b,t)}$ is the attitude matrix that transforms coordinates from F_t to F_b. The term $\widehat{A}^{b,t}$ denotes $\widehat{A}\left(\bar{q}^{(t/b)}\right)$ matrix. $\tilde{w}_{b/i}{}^{(b)}$ is the cross-product matrix of $\bar{w}_{b/i}{}^{(b)}$ that can be computed as

$$\tilde{w}_{b/i}{}^{(b)}=\begin{bmatrix} 0 & -w_z & w_y \\ w_z & 0 & -w_x \\ -w_y & w_x & 0 \end{bmatrix} \tag{3.3}$$

which is the cross-product matrix of $\bar{w}_{b/i}{}^{(b)}$, as used in Equation (2.13).

3.2 Controller

3.2.1 Attitude controller

The task of the control function is to set the attitude of the satellite to a desired value determined with respect to the reference frame. Attitude Controller calculates the desired amount of torque from the actuator using the desired attitude and angular velocity parameters. For attitude control, we propose a PD type controller where the parameters K_p and K_d are chosen with population-based optimization algorithm called Sine Cosine Algorithm (SCA) (Mirjalili, 2016).

In attitude control problem, the objective is to minimize the integral of the saturated quaternion error while keeping the controller parameters in a practical range. The optimization problem can be formulated as follows

$$\text{minimize } \int_0^{100} \left(\bar{q}_{err}{}^{(b/i)}\right)^2 dt \tag{3.4}$$

$$\text{subject to } K_p, K_d \leq 50000 \; K_p, K_d \geq 1$$

where $\bar{q}_{err}{}^{(b/i)}$ is the saturated quaternion error.

3.2.1.1 Pole placement method

Pole placement technique can be used to place the closed-loop eigenvalues at any desired location. In this study, we use the pole placement method for attitude controller of the satellite. The proportional and derivative gains of the attitude controller, denoted by K_p and K_d respectively, are calculated with this method.

$$w_n = \frac{4}{T_s \xi} \tag{3.5}$$

where ξ is the damping ratio and T_s is the settling time.

Closed loop nonlinear systems of a rigid body satellite with a PD control logic is globally asymptotically stable for the following gain K_g selection according to (Wie, 1998)

$$K_g=(2\hat{J}_s^{(b)})^{-1} \tag{3.6}$$

where $\hat{J}_s^{(b)}$ is the satellite inertia matrix. K_p and K_d are formulated as follows

$$K_p=K_g^{-1}w_n^2 \tag{3.7}$$

$$K_d=K_g^{-1}(2\xi w_n) \tag{3.8}$$

3.2.1.2 Reaction wheel angular momentum calculation

The internal and external torques applied to the satellite must be controlled in order to control attitude and keep the angular velocity of the satellite at the desired value. Angular momentum of the reaction wheels along their spin axes can be written as

$$\bar{H}_w^{(b)}=\sum_{i=1}^{n_{wheel}} J_{wi}\, w_{wi/b}\bar{u}_{wi}^{(b)}. \tag{3.9}$$

Due to non-periodic and accumulated disturbing torques, the reaction wheels reach their momentum limit values and cannot generate more torque. Because of this, satellite cannot ensure the attitude. Therefore, the momentum unloading of the reaction wheels is required to compensate this disturbance torques. Torque command is given to the thrusters to reduce the speed of the reaction wheels. Control torque distributed to thrusters is calculated as

$$\bar{u}_c^{(b)}=K_p\bar{q}_{err}^{(b/i)}-K_d\bar{w}_{b/t}^{(b)}-\tilde{w}_{b/i}^{(b)}(\hat{J}_s^{(b)}\bar{w}_{b/i}^{(b)}+\bar{H}_w^{(b)}). \tag{3.10}$$

Obtained torque is distributed to the six thrusters in the Thruster Allocation block shown in **Figure 2.5**.

3.2.2 Wheel speed controller

The wheel speed controller keeps the reaction wheel speed at a predetermined value. The block shown at the bottom of the **Figure 2.5** illustrates the reaction wheel control mechanism. IP type controller is used to bring the wheels to the desired speed. IP controller is an advanced form of PI controller where the integral part is in the feedforward path and the proportional part is in feedback path. This controller does not result in high overshoot as opposed to the conventional PI controller. Note here that the anti-windup part prevents integration wind-up in IP controller to eliminate the windup problem. The wheel speed controller diagram is depicted in **Figure 3.1**.

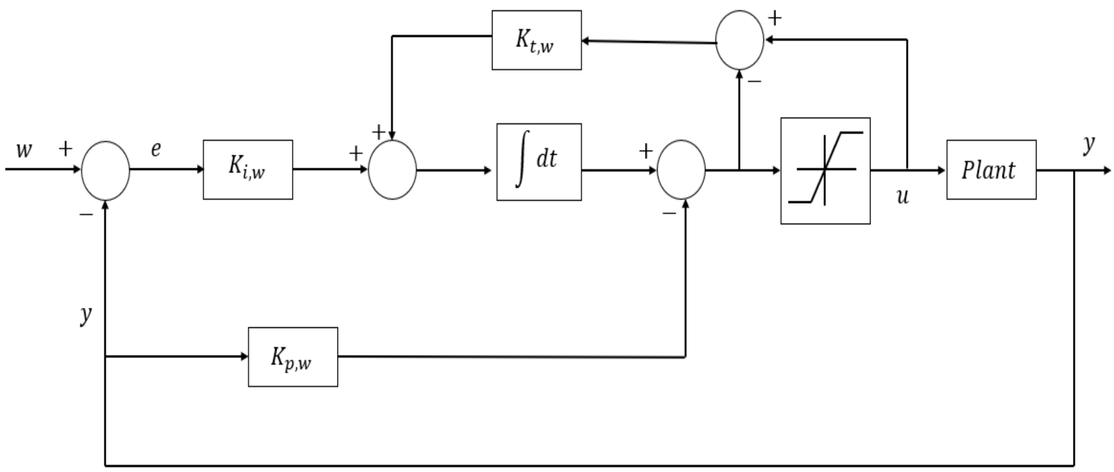

Figure 3.1 Integral Anti Windup for IP Controller Diagram

As can be seen from **Figure 3.1**, w is the reaction wheel speed that is obtained from the attitude dynamics. Here, u is the reaction wheel torque, $K_{i,w}$ is the wheel speed controller integral gain, $K_{p,w}$ is the wheel speed controller proportional gain, and $K_{t,w}$ is the wheel speed controller anti-windup gain.

3.3 Optimization Problem

3.3.1 Sine cosine algorithm

Sine-Cosine Algorithm (SCA) is a population-based heuristic optimization technique proposed by (Mirjalili, 2016) to solve optimization problems. SCA is based on sine cosine mathematical functions and uses these functions for exploration and exploitation of the search space to find the best solution.

SCA initially generates multiple random solutions. Several random and adaptive variables are integrated into the algorithm to strengthen the exploration and exploitation phases. The position update equations for SCA include these phases in the update formula as follows

$$X_i^{t+1} = \begin{cases} X_i^t + r_1 \times \sin(r_2) \times \left| r_3 P_i^t - X_i^t \right|, \ r_4 < 0.5 \\ X_i^t + r_1 \times \cos(r_2) \times \left| r_3 P_i^t - X_{ii}^t \right|, r_4 \geq 0.5 \end{cases} \tag{3.11}$$

where X_i^t is the position of the current solution in i-th dimension at t-th iteration, P_i^t is position of the target point in i-th dimension at t-th iteration, and r_2, r_3, r_4 are random numbers with $r_4 \in [0,1]$.

In the above pair of equations, r_1 defines the next location region. It could be located either inside or outside the space between target and solution. r_2 determines how far the movement is towards or away from the target point. r_3 defines a random weight for the target and stochastically increases ($r_3 > 1$) or decreases ($r_3 < 1$) the effect of the target point in determining distance. Lastly, r_4 provides an equal transition from the sine function to cosine function or vice versa in Equation (3.11).

The SCA algorithm has superior exploration and exploitation ability. Moreover, it escapes from the local optimum, and it converges quickly to the global optimum. Also, it is not affected by the structure of the problem. The range of sine and cosine functions in Equation (3.11) are adaptively adjusted with the given formula in Equation (3.12) to balance the exploration and exploitation stages of the algorithm. The parameter r_1 is defined as

$$r_1 = b - k\frac{b}{K} \tag{3.12}$$

where k is the current iteration, K is the maximum number of iterations, and b is a constant.

3.3.2 Convex optimization algorithm

In this study, we use convex optimization to solve the thruster allocation problem by assuring global optimum solutions. The method for solving a nonlinear constrained quadratic optimization problem that can be formulated as

$$\begin{aligned} &\text{minimize: } f(y) \\ &\text{subject to: } h(y)=0, \\ &y \geq 0 \end{aligned} \tag{3.13}$$

The cost function and the constraints can be rewritten as

$$f(y) = \frac{1}{2} y^T y \tag{3.14}$$

$$h(y) = A_u y - u = 0 \tag{3.15}$$

where

$$u = \begin{bmatrix} F \\ \bar{u}_c^{(b)} \end{bmatrix} \tag{3.16}$$

is the desired thrust vector, F is the force generated in the maneuver direction (F_x or F_y), y is the thrust force vector. A_u is the 4×6 allocation matrix formed according to the maneuver direction.

The optimization problem aims to minimize fuel consumption with limited thruster usage. For instance, if the satellite performs the East maneuver, ${u_{ti,x}}^{(b)}$ component of the ${u_{ti}}^{(b)}$ will be used. In this case, A_u can be written as

$$A_{u,i}=F_{max}\begin{bmatrix} {u_{ti,x}}^{(b)} \\ \bar{r}_{ti}^{(b)}\times{\bar{u}_{ti}}^{(b)} \end{bmatrix} \tag{3.17}$$

where F_{max} is the maximum allowable thrust, ${u_{ti,x}}^{(b)}$ is the x component of the i-th thruster unit vector, and $\bar{r}_{ti}^{(b)}$ is position of the i-th thruster as given in **Table 4.2**. $\bar{r}_{ti}^{(b)}\times{\bar{u}_{ti}}^{(b)}$ denotes the torques provided by i-th thruster.

The optimization algorithm guarantees global optimum solutions which provide proper thruster usage. The forces and torques provided by thrusters can be computed as

$$\begin{gathered} {\bar{F}_t}^{(b)}=F_{max}\sum_{i=1}^{6}{\bar{u}_{ti}}^{(b)}\,y \\ {\bar{T}_t}^{(b)}=F_{max}\sum_{i=1}^{6}\bar{r}_{ti}^{(b)}\times{\bar{u}_{ti}}^{(b)}y \end{gathered} \tag{3.18}$$

Using ${\bar{T}_t}^{(b)}$ and ${\bar{F}_t}^{(b)}$ one can obtain Equation (2.13) and Equation (2.11), respectively.

4 SIMULATIONS

The simulations are performed to verify the efficiency of the optimization algorithm in terms of the ability to keep satellite within a station-keeping window of ±0.01 degrees longitude and ±0.05 degrees latitude, while the maximum errors in the Euler angles (roll, pitch, yaw) are ±0.05 degrees. The attitude of the satellite with respect to F_i at the beginning of the simulation is produced with 2-1-3 Euler series angles. Therefore, the quaternion is produced without any singularity. The mass of the satellite is chosen as m=1875 kg, center of mass CoM=$[0,0,2]^T$ m, and the inertia of the satellite is

$$\hat{J}_s^{(b)}=\begin{bmatrix} 10000 & 0 & 0 \\ 0 & 5000 & 0 \\ 0 & 0 & 9000 \end{bmatrix}.$$

The initial satellite states are listed in **Table 4.1**. The satellite is propelled by six thrusters whose positions are given in **Table 4.2**. For practical reasons, we restrict the magnitude of the thrusts to be at most F_{max}=10N. In this simulation, the satellite performs the east maneuver and F_x=15N. The attitude of the satellite is controlled by four reaction wheels. The speed range of the reaction wheels are assumed to be equal to ±4500rpm. Inertia of the reaction wheels about their spin axis is chosen as $J_{w/wi}$= 0.1kgm^2. The torque range of the reaction wheels is ±0.22 Nm. In order to solve the differential equations related with satellite attitude and orbital dynamics, Runge-Kutta 4 method is used with a step size of 0.05 s.

Table 4.1 Initial satellite states

Satellite position in F_i (km)	-3396.7311	42037.9430	-32.3488
Satellite velocity in F_i (km/s)	-3.0637	-0.2487	0.0024
Target position in F_e (km)	4700	4200	0
Attitude Roll-Pitch-Yaw (deg)	85.3589	89.4571	-90.5866
Rates (deg/sec)	0	-0.0042	0
RW Speeds (rpm)	RW1	-1200	
	RW2	-1000	
	RW3	-1000	
	RW4	-1200	

Table 4.2 Positions of the thrusters

Thruster	Position in F_e (m)
1	$\bar{r}_{t1}$=[0,-1, 0]
2	$\bar{r}_{t2}$=[0 ,-1, 4]
3	$\bar{r}_{t3}$=[-1,-1, 4]
4	$\bar{r}_{t4}$=[-1, 1, 0]
5	$\bar{r}_{t5}$=[1,-1,0]
6	$\bar{r}_{t6}$=[1, 1, 4]

4.1 East Maneuver with SCA Algorithm

The optimal attitude control gains are calculated using SCA as

K_p=diag[1890.7,4005,878.5] and K_d= diag[1499.1,1483.9,903.7] which yields T_s=[7.04 3.29 9.14]^T and ξ=0.707. Wheel speed control gains are chosen as $K_{p,w}$= 0.457, $K_{i,w}$= 0.459 and $K_{t,w}$= 10.47.

4.2 East Maneuver with Pole Placement Method

The optimal attitude control gains are calculated using pole placement method as $K_p=10^4\times$diag[1.59021,3.64088,0.85019] and $K_d= 10^4\times$diag[1.26084,1.34903,0.87461].

Wheel speed control gains are chosen as $K_{p,w}$= 0.457, $K_{i,w}$= 0.459 and $K_{t,w}$= 10.47.

First simulation performs east maneuver with the parameters are obtained from the SCA optimization procedure discussed in Section 3.3.1. **Figure 4.1a** shows that the reaction wheels reach the desired speeds. The speed of the reaction wheels is fixed to -100 rad/sec=954.92 rpm as can be seen from **Table 4.1** and the initial speeds of RW1 and RW4 are -1200 rpm. Because of this, RW1 and RW4 reach the desired speeds in a longer time than RW2 and RW3. **Figure 4.1b** shows the torques of the reaction wheels. As can be seen from the figure, torques are approaching zero, which means that the momentum of the reaction wheels is unloaded. Due to the friction torques of the wheel, torques are not definitively zero. Furthermore, **Figure 4.1c** illustrates the thrusters torque commands from the attitude controller in the x, y, and z axes.

Second simulation performs east maneuver with the parameters are obtained from the pole placement method. The speed of the reaction wheels is fixed to same value with the first simulation. **Figure 4.2a** shows that the reaction wheels reach to desired speeds. The initial speed of the reaction wheels is given in the **Table 4.1**. **Figure 4.2b** shows torques of each reaction wheel. As can be seen from the figure, torques are approaching zero, which means that the momentum of the reaction wheels is unloaded. Due to the friction torques of the wheel, torques are not definitively zero. Furthermore, **Figure 4.2c** illustrates the thrusters torque commands from the attitude controller in the x, y, and z axes.

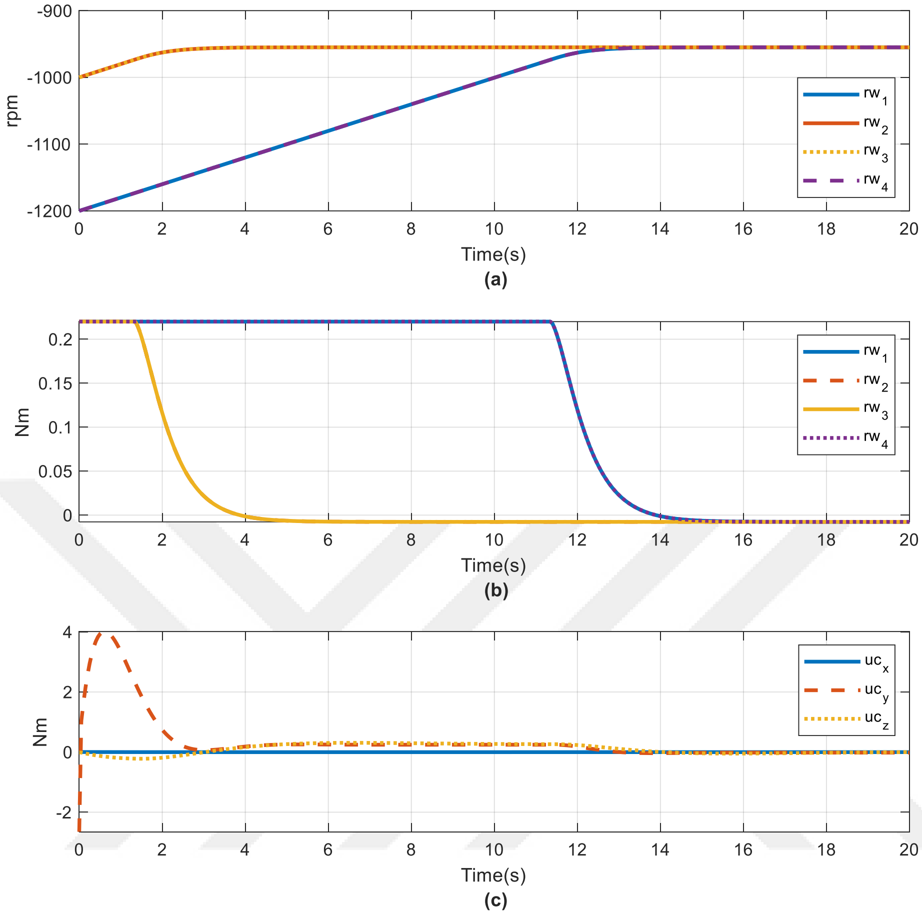

Figure 4.1 a) RW speed **b)** RW torque command **c)** Thruster torque command (with SCA parameters)

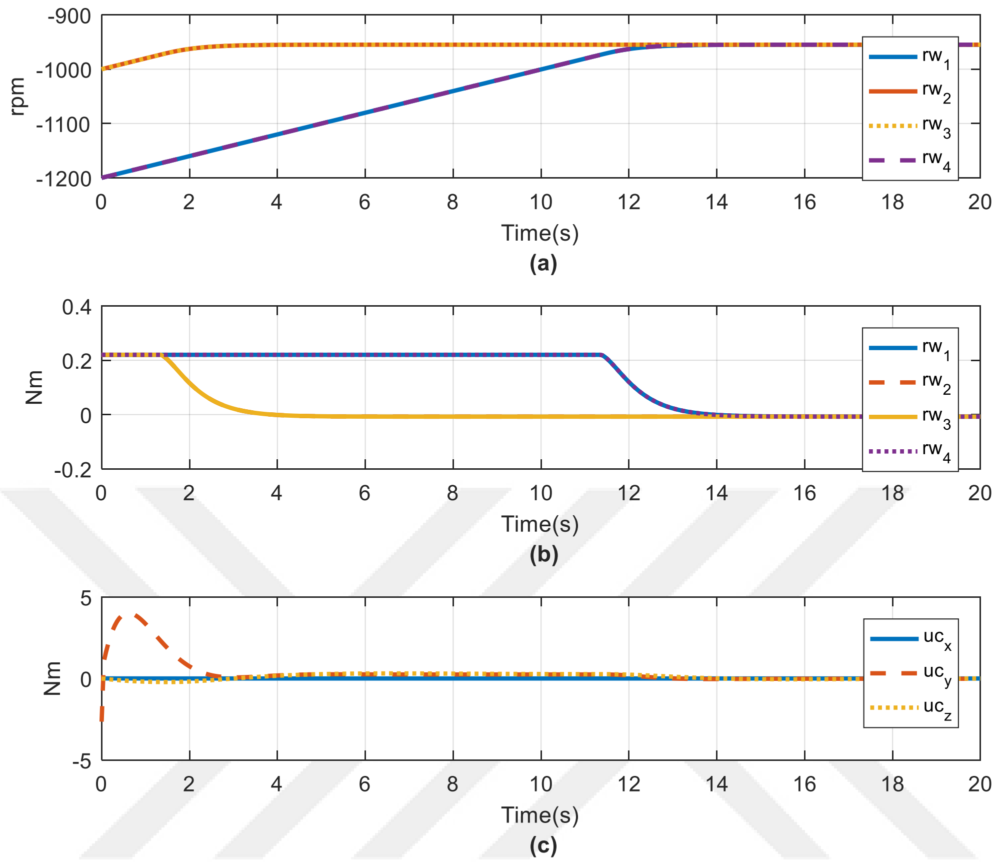

Figure 4.2 a) RW speed **b)** RW torque command **c)** Thruster torque command (obtained from the pole placement method)

Figure 4.3 shows the quaternion error as a function of time for the first simulation. As can be observed, quaternion error is within acceptable limits for a GEO satellite. **Figure 4.4** shows the quaternion error as a function of time for the second simulation. According to east maneuver simulation results using SCA algorithm, following equation is calculated as

$$\int_0^{20} \left(\bar{q}_{err}^{(b/i)}\right)^2 dt = 1.336\times10^{-6}$$

On the other hand, according to east maneuver simulation results using pole placement method, following equation is calculated as

$$\int_0^{20} \left(\bar{q}_{err}^{(b/i)}\right)^2 dt = 1.419\times10^{-6}$$

These results shows that although both results are in the acceptable limits, SCA algorithm provides a better solution than the pole placement method in terms of the integral square error of the quartenion.

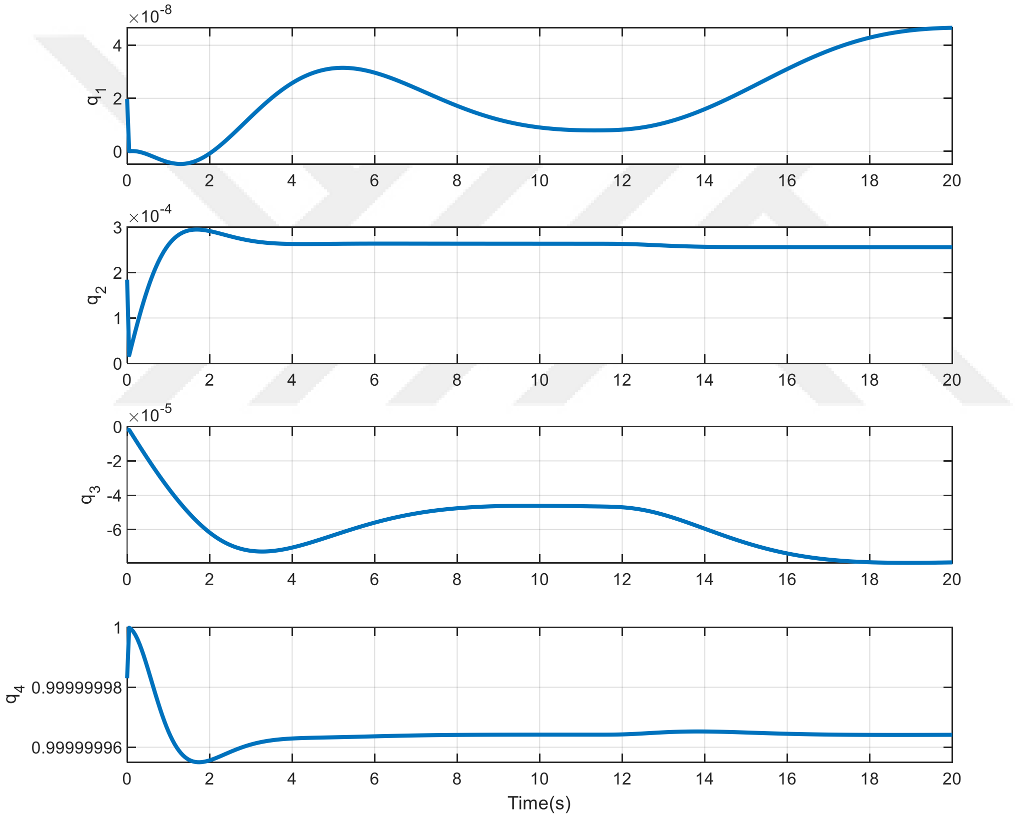

Figure 4.3 Quaternion error (with SCA parameters)

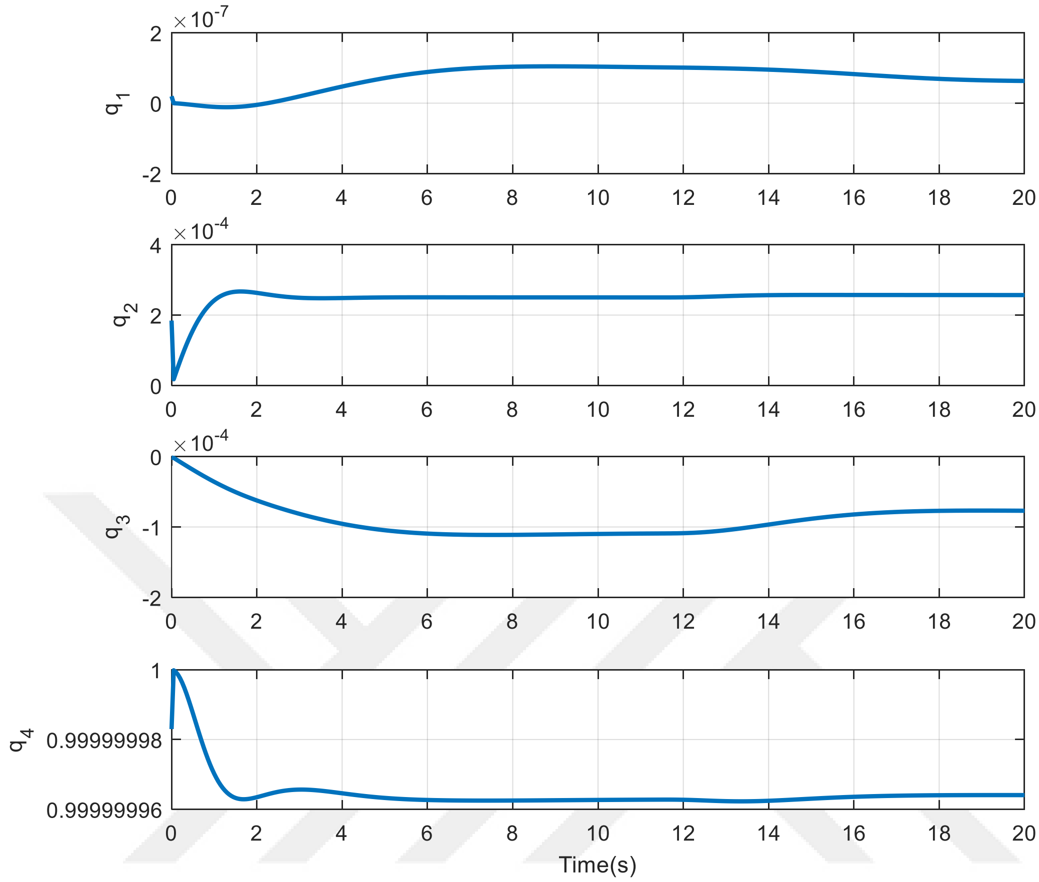

Figure 4.4 Quaternion error (obtained from the pole placement method)

Roll-pitch-yaw error angles in the first simulation are depicted in **Figure 4.5a** which shows that the constraints on the error angles are satisfied. **Figure 4.5b** shows the satellite angular rates.

Roll-pitch-yaw error angles in the second simulation are depicted in **Figure 4.6a** which shows that the constraints on the error angles are satisfied. **Figure 4.6b** shows the satellite angular rates.

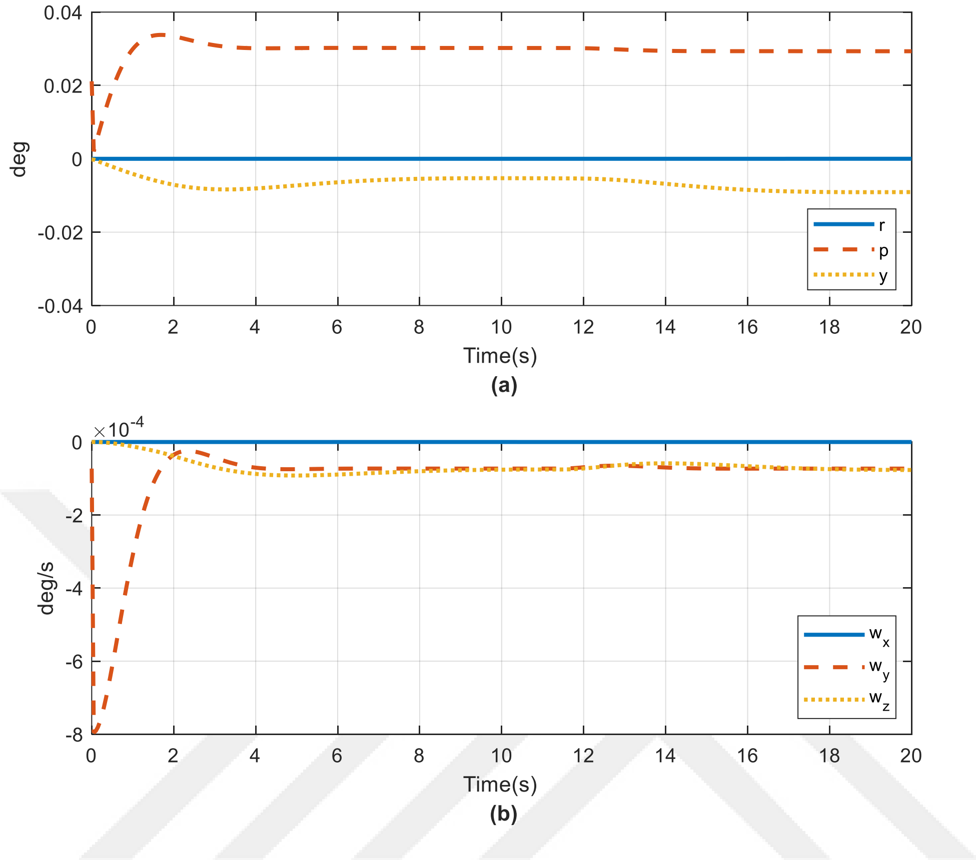

Figure 4.5 The errors in **a)** Euler angles, **b)** Angular velocity (with SCA parameters)

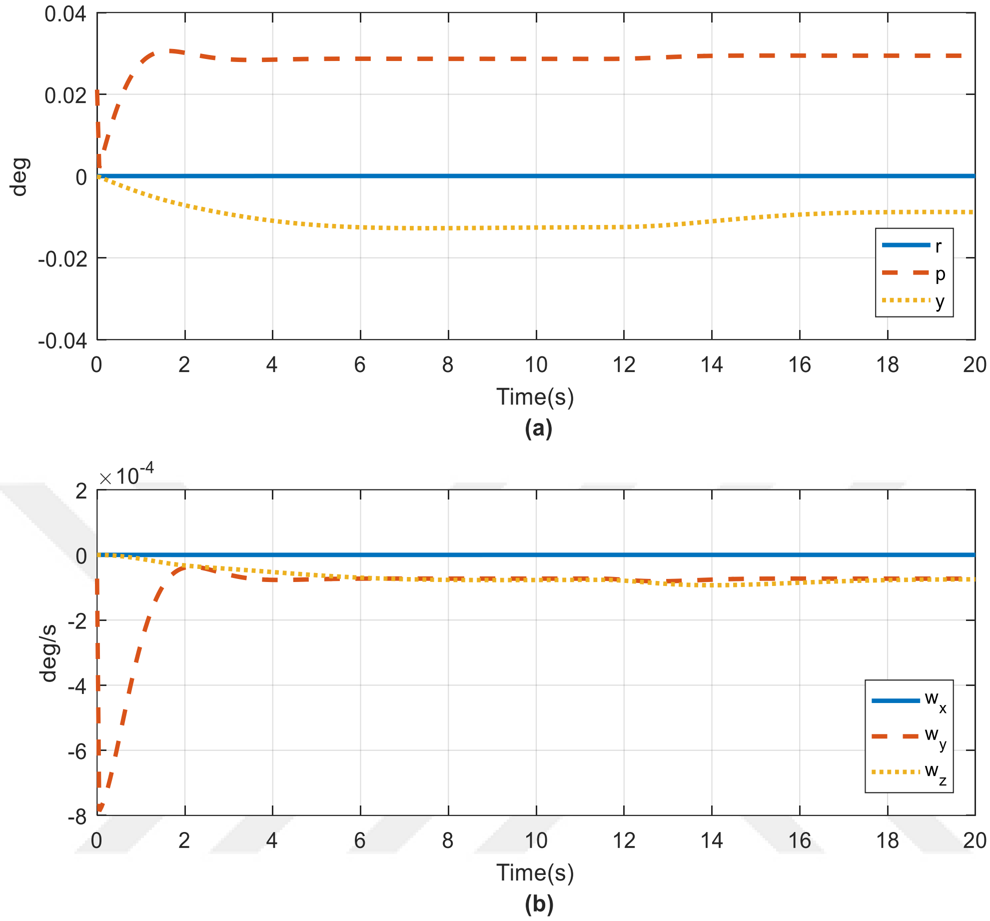

Figure 4.6 The errors in **a)** Euler angles, **b)** Angular velocity (obtained from the pole placement method)

5 CONCLUSIONS

In this thesis, a control allocation method is suggested to maintain the orbital accuracy and attitude control. The optimal control parameters that reduce the use of chemical thrusters in GEO satellites have been obtained. This study has examined the concept of GEO satellites, station-keeping maneuver types, reaction wheel speed control, attitude control, some optimization techniques. The attitude and orbital dynamics of the satellite are presented. Attitude dynamics are considered with reaction wheels. The reaction wheel speed controller ensured that the reaction wheel speeds are kept at the desired speed. Reaction wheel and chemical thruster configurations are given. The capabilities provided by the proposed configurations are discussed. In this thesis, four reaction wheels and six chemical thrusters are used. East/west and north/south maneuver strategies are examined. The north/south maneuvers are performed to correct the eccentricity of the orbit. The necessary formulas for modeling the perturbations of the satellite are given. With the methods proposed in this thesis, the satellite is maintained to point to an area on Earth while ensuring both orbital correction and momentum unloading. The fuel consumption performance is achieved with the proposed control allocation method. The reaction wheel speed controller has allowed the unload the momentum from the reaction wheels. Numerical simulations show the effectiveness of the method. We believe that the findings of the thesis are useful to understand the station-keeping concept of the GEO satellites.

REFERENCES

Borissov, S., Wu, Y., Mortari, D. (2015). East-west GEO station-keeping with degraded thruster response. Aerospace Journal, 2, 581-601.

Bruijn, F., Theil, S. (2016). Geostationary satellite station-keeping using convex optimization. Journal of Guidance, Control, and Dynamics, 39(3).

Chao, C. C., Baker, J. M. (1983). On the propagation and control of geosynchronous orbits. Journal of the Astronautical Sciences, 31, 99-115.

Curtis, H. (2010). Orbital Mechanics for Engineering Students. Daytona Beach Florida: Butterworth-Heinemann.

Emma, B. P., Pernicka, H. J. (2003). Algorithm for autonomous longitude and eccentricity control for geostationary spacecraft. Journal of Guidance, Control, and Dynamics, 26(3), 483-490.

Guelman, M. M. (2014). Geostationary satellites autonomous closed loop station keeping. Acta Astronautica, 9-15.

Ismail, Z., Varatharajoo, R. (2009) A study of reaction wheel configurations for a 3-axis satellite attitude control. Advances in Space Research, 45, 750-759.

Jin, J., Park, B., Park, Y., Tahk., M. (2006) Attitude control of a satellite with redundant thrusters. Aeorospace Science and Technology, 10, 644-651.

Kimbrel, M. S. (2002). Optimization of Electric Propulsion Orbit Raising, M.Sc. Thesis, MIT, Cambridge, MA, USA, 1-7.

Losa, D. (2007). High vs Low Thrust Station Keeping Maneuver Planning for Geostationary Satellites. PhD Thesis, Paris: École Nationale Supérieure des Mines de Paris.

Maral, G., Bousquet, M., Sun, Z. (2009). Satellite Communications Systems: Systems, Techniques and Technology, 5th, Wiley & Sons, UK.

Markley, F. L., Crassidis, J. L. (2014). Fundamentals of Spacecraft Attitude Determination and Control. Springer, New York, USA.

Mirjalili, S. (2016). SCA: A sine cosine algorithm for solving optimization problems. Knowledge-Based Systems, 96, 120-133.

Özgören, M. K. (2007). Kinematic analysis of spatial mechanical systems using exponential rotation matrices. Journal of Mechanical Design, 129, 1144-1152.

Park, B., Tank, M., Bang, H., Park, C., Jin, J. (2005). A new approach to on-board stationkeeping of GEO-satellites. Aerospace Science and Technology, 722-731.

Rex, D., Köhnecket, B. (2012). Redundant configuration of electric propulsion systems for stationkeeping. The Journal of American Institute of Aeronautics and Astronautics, 11(7), 488-500.

Satpute, S., Emami, M. R. (2019). Concurrent station keeping and momentum management of geostationary satellites. The Journal of the Astronautical Sciences, 66, 341-360.

Shrivastava, S. K. (1978). Orbital perturbations and stationkeeping of communication satellites. American Institute of Aeronautics and Astronautics, 15(2), 67-78.

Thomas, D. (2016). A Comparison of GEO Satellites Using Chemical and Electric Propulsion, http://www.colorado.edu.

Thopil, G. A. (2006) An Attitude and Orbit Determination and Control System for a small Geostationary Satellite. M.Sc. Thesis, Stellenbosch University, Stellenbosch, South Africa, 20-30.

Tsiotras, P., Shen, H., Hall, C. (2001) Satellite attitude control and power tracking with energy/momentum wheels. Journal of Guidance, Control, and Dynamics, 24(1).

Vallado, D. A. (2001). Fundamentals of Astrodynamics and Applications, 2nd Edition, Kluwer Academic Publishers, Dordrecht, Holland.

Weiss, A., Kalabic, U. V., & Cairano, S. D. (2018). Station keeping and momentum management of low-thrust satellites using MPC. Aerospace Science and Technology, 76, 229-241.

Wertz, J. R. (1998). Spacecraft Attitude Determination and Control, Kluwer Academic Publishers, Dordrecht, Holland.

Wie, B. (1998). Space Vehicle Dynamics and Control, American Institute of Aeronautics and Astronautics, Inc., Reston, VA.

Yılmaz, Ü. C. (2016). Design and Performance Improvement of LEO-GEO Ground Station Communication System: Turkey Example, PhD Thesis, Karadeniz Technical University, Trabzon, Turkey, 40-45.